



Mathematically established chaos and forecast of statistics with recurrent patterns in Taylor–Couette flow

B. Wang¹ , R. Ayats¹ , K. Deguchi² , A. Meseguer³  and F. Mellibovsky³ 

¹Institute of Science and Technology Austria (ISTA), Klosterneuburg 3400, Austria

²School of Mathematics, Monash University, Clayton, VIC 3800, Australia

³Departament de Física, Universitat Politècnica de Catalunya, Barcelona 08034, Spain

Corresponding authors: K. Deguchi, kengo.deguchi@monash.edu; F. Mellibovsky, fernando.mellibovsky@upc.edu

(Received 27 December 2024; accepted 22 January 2025)

The transition to chaos in the subcritical regime of counter-rotating Taylor–Couette flow is investigated using a minimal periodic domain capable of sustaining coherent structures. Following a Feigenbaum cascade, the dynamics is found to be remarkably well approximated by a simple discrete map that admits rigorous proof of its chaotic nature. The chaotic set that arises for the map features densely distributed periodic points that are in one-to-one correspondence with unstable periodic orbits (UPOs) of the Navier–Stokes system. This supports the increasingly accepted view that UPOs may serve as the backbone of turbulence and, indeed, we demonstrate that it is possible to reconstruct every statistical property of chaotic fluid flow from UPOs.

Key words: chaos, Taylor–Couette flow, rotating turbulence

1. Introduction

About half a century ago, deterministic chaos theory revolutionised our understanding of why fluid flows are so challenging to predict, with groundbreaking contributions such as Lorenz (1963). Since then, the application of dynamical systems theory to fluid phenomena has developed into a rich and fruitful field (Eckmann 1981; Argyris, Faust & Haase 1993). However, a significant divide persists between chaos theory and statistics-based turbulence theory. To help bridge this gap, this paper examines a specific

flow pattern in the Taylor–Couette system – a classic fluid set-up extensively studied in theory, experiments and numerical simulations.

One of the major challenges of turbulence resides in understanding the mechanisms that produce coherent vortical structures, which low-dimensional models struggle to fully represent. With advancements in computational power, dynamical systems theory analyses based on numerically solving the Navier–Stokes equations have gained momentum. In the context of shear flows, research along these lines has enabled significant progress in the understanding of the physical mechanisms that govern subcritical transition to turbulence (Kerswell 2005; Eckhardt *et al.* 2007). Invariant solutions, typically in the form of travelling waves or unstable periodic orbits (UPOs), enact a fundamental part (see, for example, Nagata 1990; Clever & Busse 1997; Itano & Toh 2001; Kawahara & Kida 2001; Faisst & Eckhardt 2003; Waleffe 2003; Wedin & Kerswell 2004; Pringle, Duguet & Kerswell 2009; Mellibovsky & Meseguer 2009; Gibson, Halcrow & Cvitanovic 2009; Deguchi, Meseguer & Mellibovsky 2014).

Subsequently, the motivation for finding UPOs shifted towards understanding fully developed turbulence (Kawahara, Uhlmann & van Veen 2012; Suri *et al.* 2020; Graham & Floryan 2021; Yalnız, Hof & Budanur 2021; Crowley *et al.* 2022; Page *et al.* 2024), reviving Hopf’s original idea of using recurrent patterns (Hopf 1948). The UPOs potentially offer a promising path towards comprehending turbulence, as they provide a deterministic representation of coherent structure dynamics. However, the challenge of relating the statistical properties of turbulence to UPOs remains an open problem. While recent studies have shown that turbulent trajectories can be approximated by combinations of UPOs (Yalnız *et al.* 2021; Page *et al.* 2024), such approximations rely on *a posteriori* tuning of weighing parameters. Cycle expansion theory (Artuso, Aurell & Cvitanović 1990; Christiansen, Cvitanović & Putkaradze 1997) is the only known systematic method for deducing statistical quantities of a deterministic system exhibiting stochastic dynamics from the deterministic properties of its UPOs, but it has yet to be applied successfully to fluid systems.

Hopf’s idea was not immediately accepted because relating deterministic recurrent patterns with the inherently probabilistic nature of turbulence statistics appears rather counterintuitive. However, in simple model dynamical systems, this connection is now well-established through chaos theory, which has advanced considerably since the seminal work of Li & Yorke (1975), who introduced the first mathematical definition of chaos. Among the various definitions of chaos currently in use, Devaney’s is the most widely spread (Devaney 2022) despite being harder to prove than Li–Yorke’s (Aulbach & Kieninger 2001). A key insight from Devaney’s definition is that unstable periodic points are densely distributed within the chaotic set. Accordingly, embracing Hopf’s proposition is mathematically analogous to approximating real numbers (turbulence) with rational numbers (UPOs). This paper exposes the phenomenon in the most direct way possible for a fluid system.

The paper is structured as follows. Section 2 presents the formulation of the Taylor–Couette problem. Section 3 demonstrates that a discrete map, which excellently approximates the flow dynamics, exhibits chaos in the Li–Yorke sense. Section 4 establishes that the map is, in fact, chaotic in the sense of Devaney. In this section, we reconstruct the statistical properties of fluid chaos from those of UPOs, independently of direct numerical simulation (DNS) data. Finally, § 5 concludes the paper.

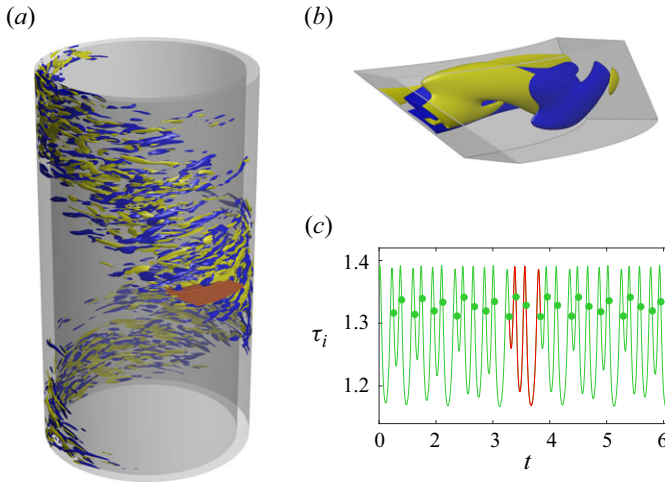


Figure 1. Taylor–Couette problem. (a) The spiral turbulence regime visualised by isosurfaces of azimuthal vorticity. The small parallelogram-annular domain in orange is the minimal flow unit used throughout this paper, adopted from Wang *et al.* (2022). (b) Snapshot of the P₃ solution in the minimal flow unit at a value of the inner cylinder Reynolds number $R_i = 395.7816$ (see definition in the text). (c) The DNS time signal of inner torque τ_i . Circles denote crossings of the Poincaré section Σ . The red portion indicates a transient approach to P₃.

2. Minimal box computation for the Taylor–Couette system

We target in our investigation the counter-rotating regime of Taylor–Couette flow, known for the subcritical onset of seemingly chaotic dynamics. The emergence of alternating turbulent and laminar helical bands (Coles 1965) has puzzled physicists since its discovery (Feynman 1964). These peculiar flow structures (figure 1a), which exhibit a clear-cut mean structure (Wang *et al.* 2023), act as harbingers of full-fledged turbulence (Andereck, Liu & Swinney 1986). Constraining the turbulent motions within the stripes to small computational domains of parallelogram-annular shape (the small orange box in figure 1a and the domain of figure 1b), which can be regarded as a minimal flow unit (Jimenez & Moin 1991; Hamilton, Kim & Waleffe 1995) for the small-scale structures – about the smallest that can sustain turbulence at sufficiently large rotation rates – has been recently found to significantly tame the dynamics, thereby unveiling simple solutions (Wang *et al.* 2022). In this domain, and for the right set of dynamical parameters, the route to chaos begins with a Feigenbaum cascade (Wang *et al.* 2024) as shown in figure 2(a). We shall shortly see that, some distance past the accumulation point (R_∞), an unstable period-3 orbit (P₃, red triangles) can be identified.

Our computational set-up deals with an incompressible fluid of kinematic viscosity ν confined between two coaxial cylinders of inner and outer radii r_i and r_o , respectively. The inner and outer cylinders are independently rotating with respect to their common axis at angular speeds Ω_i and Ω_o . The fluid motion is governed by the Navier–Stokes equations,

$$\partial_t \mathbf{v} + (\mathbf{v} \cdot \nabla) \mathbf{v} = -\nabla(p - zf(t)) + \nabla^2 \mathbf{v}, \quad (2.1)$$

expressed in non-dimensional form, using the radial gap $d = r_o - r_i$ and d^2/ν as units of length and time, respectively. This scaling leads to the inner, $R_i = dr_i \Omega_i/\nu$, and outer, $R_o = dr_o \Omega_o/\nu$, Reynolds numbers associated with the rotation of the inner and outer cylinders, respectively. The pressure gradient consists of two components: an axial

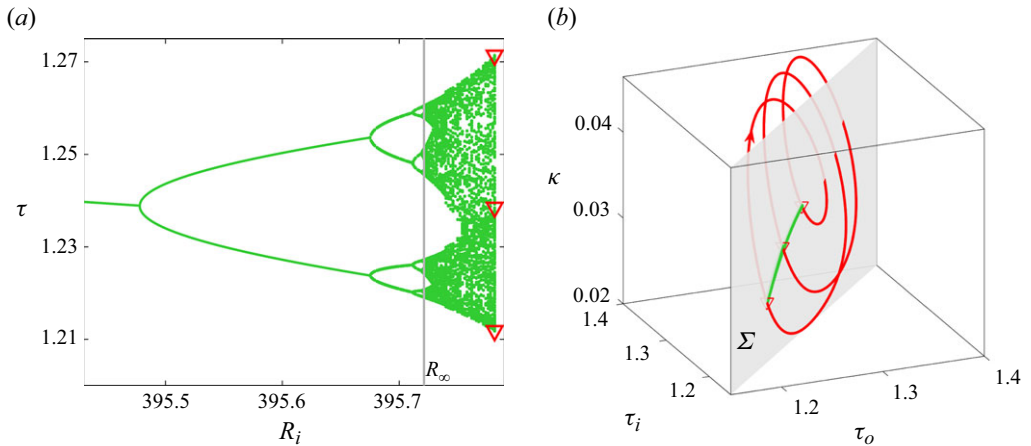


Figure 2. Attractor (from DNS data) and the period-3 orbit (converged with the Poincaré-Newton-Krylov method, PNK). (a) The bifurcation diagram generating the chaotic set. The green dots show torque τ (on the Poincaré section Σ) as a function of the inner cylinder Reynolds number R_i for statistically steady states in DNS. The red triangles indicate the period-3 orbit (P_3) at $R_i = 395.7816$, at some distance beyond the cascade’s accumulation point R_∞ . (b) Phase map projection on (τ_i, τ_o, κ) of the P_3 orbit (red line) and a representation of the chaotic attractor on the Poincaré section Σ (green dots) at $R_i = 395.7816$.

forcing term ($f\hat{\mathbf{z}}$) that adjusts instantaneously to keep zero-axial net mass flux, and the rest (∇p) that constrains the velocity (\mathbf{v}) to comply with the incompressibility condition $\nabla \cdot \mathbf{v} = 0$. For convenience, we employ cylindrical coordinates (r, θ, z) . The boundary conditions at the inner and outer cylinder walls $r = r_i$ and $r = r_o$ are $\mathbf{v} = R_i \hat{\boldsymbol{\theta}}$ and $\mathbf{v} = R_o \hat{\boldsymbol{\theta}}$. Periodicity is enforced to the rest of the boundaries of the parallelogram domain (see figure 1b, illustrated with a snapshot of P_3). In our particular set-up, the radius ratio is $\eta = r_i/r_o = 0.883$, and the outer cylinder Reynolds number is fixed at $R_o = -1200$. The transition scenario for these parameter values and increasing inner cylinder Reynolds number R_i has been thoroughly studied (Meseguer *et al.* 2009; Deguchi *et al.* 2014; Wang *et al.* 2022). The DNS is performed using a fourth-order linearly implicit (IMEX) scheme, and UPOs are computed with the Poincaré-Newton-Krylov (PNK) method detailed in Wang *et al.* (2022) and using the same numerical set-up in terms of domain shape, size and resolution.

We characterise flow states by the inner τ_i and outer τ_o cylinder torques. We also use the spatially averaged kinetic energy κ of velocity deviation from the laminar circular Couette flow whenever a third observable is necessary. All quantities are normalised by their laminar value, such that $\tau_i = \tau_o = 1$ and $\kappa = 0$ for circular Couette flow. We use the torques to define the Poincaré section as

$$\Sigma = \left\{ \tilde{\mathbf{v}} \in \mathbb{X} \mid \tau_i(\tilde{\mathbf{v}}) = \tau_o(\tilde{\mathbf{v}}), \frac{d\tau_i}{dt} > \frac{d\tau_o}{dt} \right\}, \quad (2.2)$$

where $\tilde{\mathbf{v}}$ is the velocity field \mathbf{v} , duly shifted with the method of slices (Willis, Cvitanovic & Avila 2013; Wang *et al.* 2023) to remove the degeneracy induced by the spatial drift of the solutions, both in the axial and azimuthal directions, and \mathbb{X} is the corresponding phase space. The bifurcation diagram shown in figure 2(a) records the torque, on Σ , of statistically steady states. Beyond the accumulation point of the cascade, R_∞ , the seemingly chaotic attractor forms banded structures in the bifurcation diagram that progressively widen and successively merge in pairs.

Hereafter, we will focus on $R_i = 395.7816$. The energy and torque DNS signals occasionally produce nearly periodic timestamps at this value of the parameter (figure 1c). States taken from selected pseudo-periodic lapses converge onto UPOs when fed to the PNK scheme. A phase map projection of one such UPO is shown in figure 2(b). The trajectory pierces three times the Poincaré section every period, hence our naming it P_3 (see figure 1b for a snapshot of P_3 on Σ).

3. P_3 implies chaos

It is well-known in chaos theory that for 1-D (one-dimensional) maps generated by continuous functions $f: I \rightarrow I$, where $I \subset \mathbb{R}$ is an interval, the advent of period-3 orbits holds a special significance. Specifically, as established by Li & Yorke (1975), it implies chaos in the sense that the map enhances a swift mixing of the points in the interval. Moreover, according to Sharkovskii's theorem (Sharkovskii 1964), the presence of a period-3 point entails also the existence of infinitely many periodic points.

The presence of P_3 in our system therefore renders the application of the Li–Yorke and Sharkovskii theorems highly enticing. However, the theorems hinge upon an imperative condition: the map must be 1-D and continuous. These theorems might not hold true for higher dimensional systems, even if period-3 orbits were in existence. While instances of period-3 solutions abound in the fluid dynamics literature (Moore *et al.* 1983; Knobloch *et al.* 1986; Kreilos & Eckhardt 2012), no study has positively checked, to the best of our knowledge, the conditions for the validity of these theorems.

A very long DNS (over 500 viscous time units) was conducted, with the solution $\tilde{\mathbf{v}}(t_j)$ recorded at the chronologically ordered discrete times t_j , $j = 0, 1, 2, \dots$, at which the phase map trajectory crosses the Poincaré section Σ . The approximately 2500 data points we collected are shown as green dots in figure 2(b). All points are tightly clustered on a very narrow band, akin to a 1-D curve. This holds for any projection of \mathbb{X} one might choose, which indicates a highly restricted dimensionality of the first return (Poincaré) map $\Phi: \Sigma \rightarrow \Sigma$. Strictly speaking, the dimension cannot be exactly one in the case of reversible maps but, as demonstrated by well-known examples such as the Hénon map or the Lorenz system, it can approach one. Indeed, since our system is at a relatively low Reynolds number, it is plausible that the dimension of the inertial manifold (Temam 1989; Ding *et al.* 2016; Haller *et al.* 2023) might be particularly low. Figure 3(a) shows the return map in terms of the torque $\tau(j) \equiv \tau_i(\tilde{\mathbf{v}}(t_j)) = \tau_o(\tilde{\mathbf{v}}(t_j))$. The multivaluedness of the map hinders direct application of standard 1-D dynamical systems theory, but this can be readily addressed by simple identification of the selection rule among branches. The curve in figure 3(a) is naturally split at the cusp point $\tau = \tau_c$ into two main branches: A (grey scale) and B (orange). Branch A is then further split in two sub-branches, A1 (dark) and A2 (light), for convenience. The diagram in the inset summarises the selection rule among branches. A point on branch A1 might be mapped to itself or sent to branch A2 and thence immediately to branch B. Then branch B instantly repels the trajectory, but whether A1 or A2 is to follow depends on the landing location along the branch.

A single-valued version of the map can then be constructed by applying the change of variable

$$\tilde{\tau}(j) = \begin{cases} 2\tau_c - \tau(j) & \text{if } \tau(j-1) > \tau_m \\ \tau(j) & \text{otherwise} \end{cases}, \quad (3.1)$$

where $\tau_m \approx 1.250$ is the location of the local minimum of the multivalued function, whose immediate surroundings are mapped to the vicinity of $\tau_c \approx 1.212$. This change of variable corresponds effectively to the unfolding of the map, shown in figure 3(b), which now

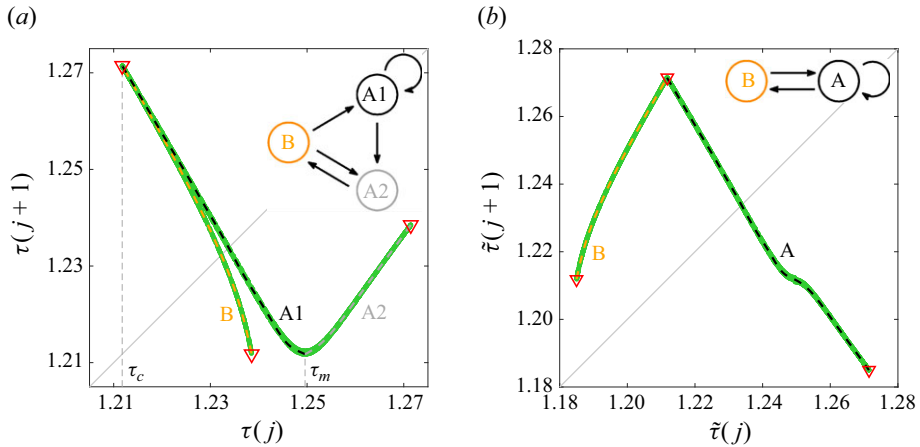


Figure 3. Return map analyses based on the Poincaré map on Σ at $R_i = 395.7816$. (a) Return map of the chaotic attractor (green dots) and of P_3 (red triangles). The cusp (τ_c) and minimum (τ_m) points split the map in three distinct branches: B (orange), A1 (black) and A2 (grey). (b) The same return map, now unfolded following (3.1). The A1 and A2 branches are now labelled as A (black). The inset diagrams in (a) and (b) indicate branch selection rules.

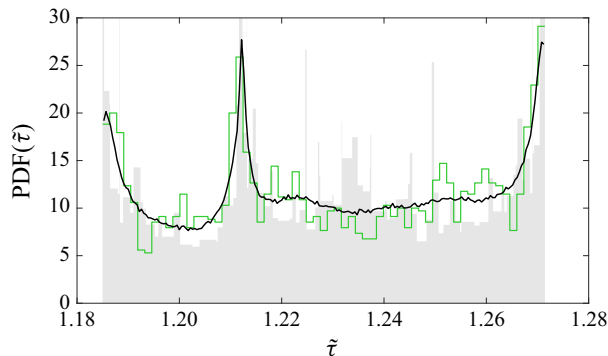


Figure 4. The PDF for the spline dynamical system (black), the normalised histogram for DNS data of the chaotic attractor (green), and the prediction from periodic points (grey).

admits standard cob-webbing to monitor the dynamics. By interpolating the DNS data points and P_3 using splines, it is possible to construct a continuous function $S : I \rightarrow I$, where $I \approx [1.185, 1.271]$. The spline dynamical system $\tilde{\tau}(j+1) = S(\tilde{\tau}(j))$ is chaotic in the Li–Yorke sense, because it contains the P_3 points, which in this case appear at the vertex and endpoints of the continuous function S .

A natural question follows regarding the extent to which iteration of the spline map reproduces DNS results, an issue that needs assessing. To this end, we compare the probability density functions (PDFs) in figure 4. The PDF corresponding to the spline dynamical system (black curve), with its Lyapunov exponent of approximately 0.47, excellently matches the DNS results (green curve). The emergence of peaks in the PDF around the period-3 points is a common feature of the intermittency route to chaos (Pomeau & Manneville 1980; Eckmann 1981).

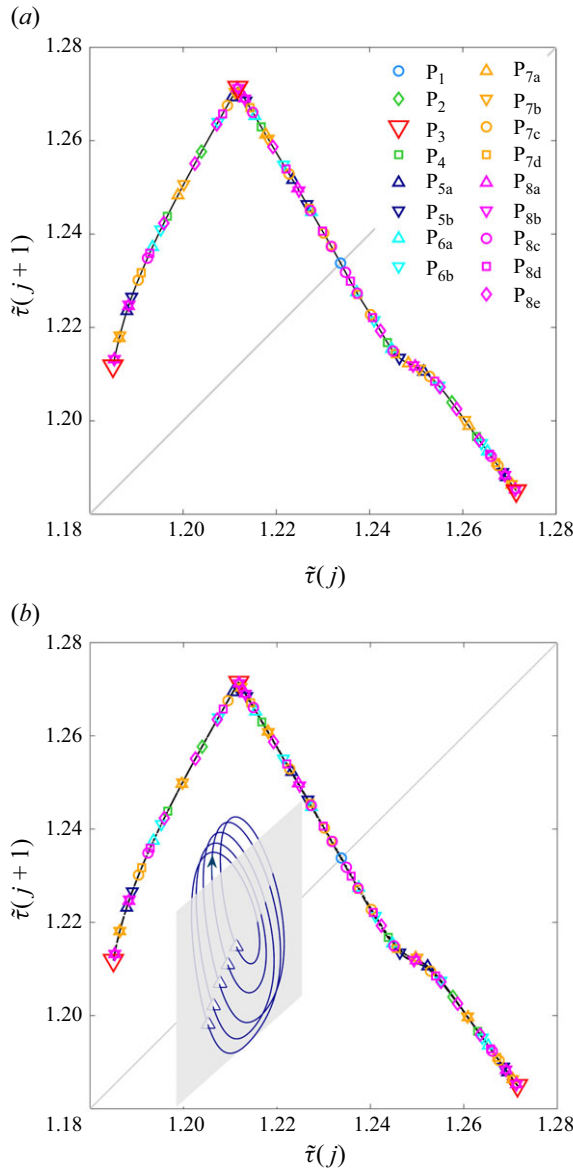


Figure 5. Complete set of periodic points up to period $n = 8$ for (a) the spline map approximation and (b) the Navier–Stokes system. The inset shows a phase map projection of P_{5a} analogous to that of P_3 in figure 3(a).

4. Probability density function computed from unstable periodic solutions

The inherent relation between the spline dynamical system and the Navier–Stokes dynamics becomes all the more evident through the comparison of periodic solutions. For the 1-D spline map, Sharkovskii’s theorem guarantees the existence of periodic points of period n for every $n \in \mathbb{N}$. Figure 5(a) shows the complete set up to $n = 8$. We have been able to find the Navier–Stokes counterpart to each and every one of the spline periodic points employing PNK (see figure 5b). The discrepancy in terms of torque between spline map and the Navier–Stokes solutions is consistently below 0.25 %.

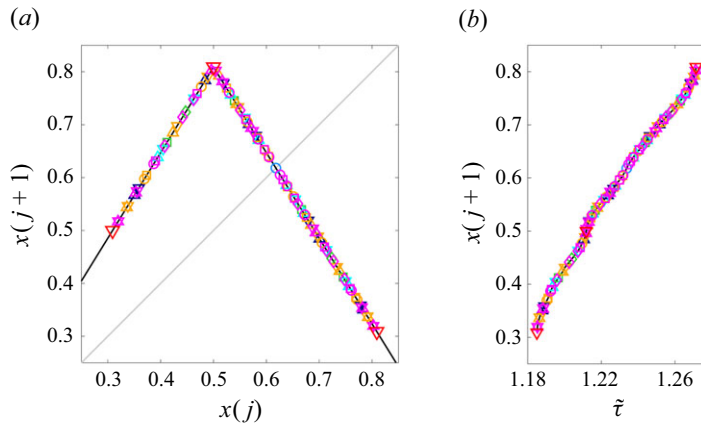


Figure 6. Topological conjugacy of the tent and spline maps. (a) The tent map $T(x)$ with all periodic points up to period $n \leq 8$. (b) Correspondence between tent map (ordinate) and spline map (abscissa) periodic points. The piecewise linear curve connecting the points provides an approximation of the conjugacy homeomorphism $h(\tilde{\tau})$. Symbols and colours, representing periodic orbits, follow the legend used in previous figures.

The fluid flow scenario we have chosen is accurately described by a map of great mathematical simplicity, whose elegant attributes make it possible to infer the PDF of chaotic dynamics from the underlying periodic points in a clear and straightforward manner. First we note that the branch selection of the unfolded map, shown in the inset of figure 3(b), is extremely simple, with B and A representing the branches to the left and right of the maximum, respectively. The diagram is nothing but the topological Markov chain over the alphabet $\{A, B\}$, whose topological entropy is known to be the natural logarithm of the golden ratio $\phi = (1 + \sqrt{5})/2$ (see Cvitanović *et al.* (2016) for the derivation). The spline map being an interval map of strictly positive entropy, one can conclude that it must be chaotic in the sense of Devaney (Li 1993; Devaney 2022). The periodic points are, therefore, densely distributed within the chaotic set, which supports the recurring assertion among fluid dynamicists that UPOs form the skeleton of turbulence (Kawahara *et al.* 2012; Graham & Floryan 2021; Crowley *et al.* 2022; Avila, Barkley & Hof 2023). The 100 periodic points we have computed cover the map effectively, thus suggesting that UPOs indeed encode the dynamics and, consequently, hold the key to predicting the statistical properties inherent to chaos.

The PDF of the spline map can be obtained from that of the tent map, $T(x) = \phi(1 - |2x - 1|)/2$, with the scale parameter tuned to induce the appropriate topological Markov chain, i.e. having the same topological entropy ϕ . Its PDF has a piecewise-constant closed analytical expression (Cvitanović *et al.* 2016):

$$\rho_T(x) = \begin{cases} \frac{2\phi}{2\phi - 1} & \text{if } \frac{\phi - 1}{2} \leq x < \frac{1}{2}, \\ \frac{2\phi}{3 - \phi} & \text{if } \frac{1}{2} \leq x \leq \frac{\phi}{2}. \end{cases} \quad (4.1)$$

Remarkably, the tent T and spline S maps share a common list of periodic solutions, appearing in the exact same order along the curve (figure 6a). This implies the existence of a homeomorphism h such that $h(S(\tilde{\tau})) = T(h(\tilde{\tau}))$, i.e. the two maps are topologically conjugate in the sense that they are dynamically equivalent (Yuan *et al.* 2000). A discrete sampling of h emerges naturally when plotting corresponding periodic points of the two

maps on the $\tilde{\tau}$ - x plane (figure 6*b*). A straightforward calculation shows that the PDF of the spline and tent maps are related by $\rho_S(\tilde{\tau}) = \rho_T(h(\tilde{\tau})|h'(\tilde{\tau})|)$, where the prime denotes ordinary differentiation. The prediction, the grey shaded region shown in figure 4, is obtained from a piecewise linear approximation of h based on the available periodic points. The agreement with the spline and DNS data are fair despite the roughness of the estimation, as attested by the accurate reproduction of the three salient peaks.

The prediction error in the PDF occurs primarily at high frequencies, thus having a small impact on the lower-order statistical moments. The expectation E and variance V of the torque computed from the PDFs are $(E, V) = (1.2294, 6.9341 \times 10^{-4})$, $(1.2288, 7.1341 \times 10^{-4})$ and $(1.2289, 6.9144 \times 10^{-4})$, for the spline dynamical system, DNS and the UPOs prediction, respectively. Replacing the spline periodic points by the Navier–Stokes UPOs yields nearly the same results, as expected from the excellent agreement exhibited by figure 5. Furthermore, the 1-D assumption of the return map implies that the PDF for the full velocity field $\tilde{\mathbf{v}}$ can be determined in a similar manner. Therefore, all widely used turbulence statistics can, in principle, be computed using UPOs.

5. Conclusion

We have analysed, in the Taylor–Couette system, a subcritical parameter regime exhibiting dynamics that can be approximated by a simple discrete map. The map has exceptionally neat mathematical properties, which allow to rigorously establish its chaotic nature as well as the existence of infinitely many UPOs. Remarkably, the fluid system and the discrete map share a common catalogue of unstable periodic solutions with the tent map, a clear indication of topological conjugacy. A sufficient number of these solutions enables the construction of a conjugacy homeomorphism, which can be used to predict the PDF to be expected from DNS.

Our informed choice of scenario purposely aims at greatly simplifying the theoretical analysis. For more general cases, the topological properties of chaotic fluid systems could be approximated by simple Markov maps (Yalniz *et al.* 2021). As demonstrated in this paper, UPOs serve precisely as the link between such Markov maps and the Navier–Stokes system. Our theory differs from cycle expansion theory (Artuso *et al.* 1990; Cvitanović & Eckhardt 1991; Christiansen *et al.* 1997; Cvitanović *et al.* 2016) and offers a more intuitive understanding of how the PDF can be constructed from UPOs. On the other hand, cycle expansion theory has the advantage of permitting the computation of statistically averaged quantities in a simpler manner by applying prescribed formulas.

A complete understanding of turbulence is still a long way off from both the applied and the mathematical stand points. Whether Hopf’s idea can be extended to high-Reynolds-number turbulence remains an open question. Furthermore, our results, depending on numerical approximations, do not guarantee that the Navier–Stokes solutions exhibit chaotic behaviour in the sense of Devaney. Nonetheless, we expect that our demonstration of how chaos theory applies to fluid flows under certain conditions will encourage future research on this important yet difficult problem.

Funding. This research is supported by the Australian Research Council Discovery Project DP230102188 and the Ministerio de Ciencia, Innovación y Universidades (Agencia Estatal de Investigación, project nos PID 2020-114043 GB-I00 (MCIN/AEI/10.13039/501100011033) and PID 2023-150029NB-I00 (MCIN/AEI/10.13039/501100011033/FEDER, UE). B.W. and R.A.’s research has been funded by the European Union’s Horizon 2020 research and innovation programme (Marie Skłodowska-Curie grant agreement no. 101034413). R.A. has also been funded by the Austrian Science Fund (FWF) 10.55776/ESP1481224.

Declaration of interests. The authors report no conflict of interest.

REFERENCES

- ANDERECK, C.D., LIU, S.S. & SWINNEY, H.L. 1986 Flow regimes in a circular Couette system with independently rotating cylinders. *J. Fluid Mech.* **164**, 155–183.
- ARGYRIS, J., FAUST, G. & HAASE, M. 1993 Routes to chaos and turbulence. A computational introduction. *Phil. Trans. R. Soc. Lond. A: Phys. Eng. Sci.* **344** (1671), 207–234.
- ARTUSO, R., AURELL, E. & CVITANOVIĆ, P. 1990 Recycling of strange sets: I. Cycle expansions. *Nonlinearity* **3** (2), 325–359.
- AULBACH, B. & KIENINGER, B. 2001 On three definitions of chaos. *Nonlinear Dyn. Syst. Theory* **1**, 23–37.
- AVILA, M., BARKLEY, D. & HOF, B. 2023 Transition to turbulence in pipe flow. *Annu. Rev. Fluid Mech.* **55** (1), 575–602.
- CHRISTIANSEN, F., CVITANOVIĆ, P. & PUTKARADZE, V. 1997 Spatiotemporal chaos in terms of unstable recurrent patterns. *Nonlinearity* **10** (55), 55–70.
- CLEVER, R.M. & BUSSE, F.H. 1997 Tertiary and quaternary solutions for plane Couette flow. *J. Fluid Mech.* **344**, 137–153.
- COLES, D. 1965 Transition in circular Couette flow. *J. Fluid Mech.* **21** (3), 385–425.
- CROWLEY, C.J., PUGUE-SANFORD, J.L., TOLER, W., KRYGIER, M.C., GRIGORIEV, R.O. & SCHATZ, M.F. 2022 Turbulence tracks recurrent solutions. *Proc. Natl Acad. Sci. USA* **119** (34), e2120665119.
- CVITANOVIĆ, P., ARTUSO, R., MAINIERI, R., TANNER, G. & VATTAY, G. 2016 *Chaos: Classical and Quantum*. Niels Bohr Institute.
- CVITANOVIĆ, P. & ECKHARDT, B. 1991 Periodic orbit expansions for classical smooth flows. *J. Phys. A: Math. Gen.* **24** (5), L237–L241.
- DEGUCHI, K., MESEGUER, A. & MELLIBOVSKY, F. 2014 Subcritical equilibria in Taylor–Couette flow. *Phys. Rev. Lett.* **112** (18), 184502.
- DEVANEY, R.L. 2022 *An Introduction To Chaotic Dynamical Systems*, 3rd edn. CRC.
- DING, X., CHATÉ, H., CVITANOVIĆ, P., SIMINOS, E. & TAKEUCHI, K.A. 2016 Estimating the dimension of an inertial manifold from unstable periodic orbits. *Phys. Rev. Lett.* **117** (2), 024101.
- ECKHARDT, B., SCHNEIDER, T.M., HOF, B. & WESTERWEEL, J. 2007 Turbulence transition in pipe flow. *Annu. Rev. Fluid Mech.* **39** (1), 447–468.
- ECKMANN, J.-P. 1981 Roads to turbulence in dissipative dynamical systems. *Rev. Mod. Phys.* **53** (4), 643–654.
- FAISST, H. & ECKHARDT, B. 2003 Travelling waves in pipe flow. *Phys. Rev. Lett.* **91** (22), 224502.
- FEYNMAN, R.P. 1964 *Lecture Notes in Physics*, vol. 2. Addison-Wesley.
- GIBSON, J.F., HALCROW, J. & CVITANOVIĆ, P. 2009 Equilibrium and travelling-wave solutions of plane Couette flow. *J. Fluid Mech.* **638**, 243–266.
- GRAHAM, M.D. & FLORYAN, D. 2021 Exact coherent states and the nonlinear dynamics of wall-bounded turbulent flows. *Annu. Rev. Fluid Mech.* **53** (1), 227–253.
- HALLER, G., KASZÁS, B., LIU, A. & AXÁS, J. 2023 Nonlinear model reduction to fractional and mixed-mode spectral submanifolds. *Chaos: Interdisciplinary J. Nonlinear Sci.* **33** (6), 063138.
- HAMILTON, J.M., KIM, J. & WALEFFE, F. 1995 Regeneration mechanisms of near-wall turbulence. *J. Fluid Mech.* **287**, 317–348.
- HOPF, E. 1948 A mathematical example displaying features of turbulence. *Commun. Pure Appl. Maths* **1** (4), 303–322.
- ITANO, T. & TOH, S. 2001 The dynamics of bursting process in wall turbulence. *J. Phys. Soc. Japan* **70** (3), 703–716.
- JIMENEZ, J. & MOIN, P. 1991 The minimal flow unit in near-wall turbulence. *J. Fluid Mech.* **225**, 213–240.
- KAWAHARA, G., UHLMANN, M. & VAN VEEN, L. 2012 The significance of simple invariant solutions in turbulent flows. *Annu. Rev. Fluid Mech.* **44** (1), 203–225.
- KAWAHARA, K. & KIDA, S. 2001 Periodic motion embedded in plane Couette turbulence: regeneration cycle and burst. *J. Fluid Mech.* **449**, 291–300.
- KERSWELL, R.R. 2005 Recent progress in understanding the transition to turbulence in a pipe. *Nonlinearity* **18** (6), R17–R44.
- KNOBLOCH, E., MOORE, D.R., TOOMRE, J. & WEISS, N.O. 1986 Transitions to chaos in two-dimensional double-diffusive convection. *J. Fluid Mech.* **166**, 409–448.
- KREILOS, T. & ECKHARDT, B. 2012 Periodic orbits near onset of chaos in plane Couette flow. *Chaos* **22** (4), 047505.
- LI, S. 1993 ω -chaos and topological entropy. *Trans. Am. Math. Soc.* **339** (1), 243–249.
- LI, T.Y. & YORKE, J.A. 1975 Period three implies chaos. *Am. Math. Mon.* **82** (10), 985–992.
- LORENZ, E.N. 1963 Deterministic nonperiodic flow. *J. Atmos. Sci.* **20** (2), 130–141.
- MELLIBOVSKY, F. & MESEGUER, A. 2009 Critical threshold in pipe flow transition. *Phil. Trans. R. Soc. Lond. A: Math. Phys. Eng. Sci.* **367** (1888), 545–560.

- MESEGUER, A., MELLIBOVSKY, F., AVILA, M. & MARQUES, F. 2009 Instability mechanisms and transition scenarios of spiral turbulence in Taylor–Couette flow. *Phys. Rev. E* **80** (4), 046315.
- MOORE, D.R., TOOMRE, J., KNOBLOCH, E. & WEISS, N.O. 1983 Period doubling and chaos in partial differential equations for thermosolutal convection. *Nature* **303** (5919), 663–667.
- NAGATA, M. 1990 Three-dimensional finite-amplitude solutions in plane Couette flow: bifurcation from infinity. *J. Fluid Mech.* **217**, 519–527.
- PAGE, J., NORGAARD, P., BRENNER, M.P. & KERSWELL, R.R. 2024 Recurrent flow patterns as a basis for two-dimensional turbulence: predicting statistics from structures. *Proc. Natl Acad. Sci. USA* **121** (23), e2320007121.
- POMEAU, Y. & MANNEVILLE, P. 1980 Intermittent transition to turbulence in dissipative dynamical systems. *Commun. Math. Phys.* **74** (2), 189–197.
- PRINGLE, C.C.T., DUGUET, Y. & KERSWELL, R.R. 2009 Highly symmetric travelling waves in pipe flow. *Phil. Trans. R. Soc. Lond. A: Math. Phys. Eng. Sci.* **367** (1888), 457–472.
- SHAROVSKIY, A.N. 1964 Co-existence of cycles of a continuous mapping of the line into itself. *Ukrainian Math. J.* **16**, 61–71.
- SURI, B., KAGEORGE, L., GRIGORIEV, R.O. & SCHATZ, M.F. 2020 Capturing turbulent dynamics and statistics in experiments with unstable periodic orbits. *Phys. Rev. Lett.* **125** (6), 064501.
- TEMAM, R. 1989 Do inertial manifolds apply to turbulence? *Physica D: Nonlinear Phenom.* **37** (1-3), 146–152.
- WALEFFE, F. 2003 Homotopy of exact coherent structures in plane shear flows. *Phys. Fluids* **15** (6), 1517–1534.
- WANG, B., AYATS, R., DEGUCHI, K., MELLIBOVSKY, F. & MESEGUER, A. 2022 Self-sustainment of coherent structures in counter-rotating Taylor–Couette flow. *J. Fluid Mech.* **951**, A21.
- WANG, B., AYATS, R., DEGUCHI, K., MELLIBOVSKY, F. & MESEGUER, A. 2024 Feigenbaum universality in subcritical Taylor–Couette flow. *J. Fluid Mech.* (accepted) arXiv: [2407.16097](https://arxiv.org/abs/2407.16097).
- WANG, B., MELLIBOVSKY, F., AYATS, R., DEGUCHI, K. & MESEGUER, A. 2023 Mean structure of the supercritical turbulent spiral in Taylor–Couette flow. *Phil. Trans. R. Soc. Lond. A: Math. Phys. Eng. Sci.* **381** (2246), 20220112.
- WEDIN, H. & KERSWELL, R.R. 2004 Exact coherent structures in pipe flow: travelling wave solutions. *J. Fluid Mech.* **508**, 333–371.
- WILLIS, A.P., CVITANOVIC, P. & AVILA, M. 2013 Revealing the state space of turbulent pipe flow by symmetry reduction. *J. Fluid Mech.* **721**, 514–540.
- YALNIZ, G., HOF, B. & BUDANUR, N.B. 2021 Coarse graining the state space of a turbulent flow using periodic orbits. *Phys. Rev. Lett.* **126** (24), 244502.
- YUAN, G., YORKE, J.A., CARROLL, T.L., OTT, E. & PECORA, L.M. 2000 Testing whether two chaotic one dimensional processes are dynamically identical. *Phys. Rev. Lett.* **85** (20), 4265–4268.